Temporal evolution of patterns and processes related to subsidence of the coastal area surrounding the Bevano River mouth (Northern Adriatic) – Italy

A. Taramelli [a,*], L. Di Matteo [b,1], P. Ciavola [c,2], F. Guadagnano [b], C. Tolomei [d,3]

[a] ISPRA Institute for Environmental Protection and Research, Via Vitaliano Brancati, 60, Rome, Italy

[b] Dipartimento di Fisica e Geologia, Università degli Studi di Perugia, Via Alessandro Pascoli s.n.c., Perugia, Italy

[c] Dipartimento di Fisica e Scienze della Terra, Università di Ferrara, via Saragat 1, 44100 Ferrara, Italy

[d] Remote Sensing Laboratory, Istituto Nazionale di Geofisica e Vulcanologia, Via di Vigna Murata, 605, 00143 Rome, Italy

Abstract

Subsidence is a widespread phenomenon in the Emilia-Romagna, particularly important along the littoral because the coastal system consists of sandy beaches and coastal wetlands, particularly in the area of the Delta Po Plain. The coasts are affected by a marked natural subsidence, because of tectonic processes and recent sediments consolidation. Since the second half of the last century, the subsidence in coastal area has increased significantly due to intense human activity, namely gas extraction and groundwater exploitation. The work presented in this paper aimed at investigating the temporal evolution of patterns and processes on a stretch of coast located between Lido di Dante and Lido di Classe, including the mouth of the Bevano river near Ravenna (Italy), using remotely sensed datasets. An innovative integration of remote sensing and monitoring method (Permanent Scatter Interferometric Synthetic Aperture Radar e PSInSAR, Small BAeline Subset e SBAS and Empirical Orthogonal Function e EOF analysis of 20 years of Landsat) has been used to study the temporal evolution of subsidence and its correlation with natural and anthropogenic causes. Results show an increase of the subsidence rates obtained for the last decade: the amount of subsidence due only to natural causes is typically a few millimetres per year, while the man-induced subsidence reaches values of several millimetres per years. Marshlands reclamation, groundwater pumping for agricultural and industrial purposes and methane extraction from gas fields near the coastline are the principal anthropogenic causes. Subsidence in combination with sea level rise will get worse inundation risk from the rivers and widens the coastal areas affected by storm surges and tidal

inundation. This makes subsidence an insidious threat having significant cumulative effects on flood risk or the integrity of water defenses and infrastructure.

Keywords: Subsidence, Coastal Areas, Remote Sensing, Permanent Scatter, Monitoring, Underground water, Vegetation.

1. Introduction

Subsidence in coastal areas and its relation to sea-level rise is a relevant geological, ecological and geomorphological process that also has implications for coastal ecosystems because it may generate increased sea-water flooding and salinisation of coastal aquifers and an instability of levees and infrastructure (Hallegate et al., 2013). Subsidence is a downward displacement of the land relative to sea level, and it often occurs in regions associated with alluvial sediments, such as a deltaic area or alluvial plain; these regions typically have thick Quaternary deposits comprised of clay and sandy loam (Chen and Rybczyk, 2005).

The holistic view of the environment that scientists apply when studying and interpreting landscape evolution is based on the principle that the scale of observations of certain physical processes determines the level at which spatial patterns of landscapes can be explained. This means that a physical process, such as subsidence may influence ecosystem functioning generating disturbance and determine perturbations or stress within the coastal vegetation growth (Temmerman et al., 2003). Disturbance and perturbation (D'Alpaos et al., 2012; Nicholls et al., 2011) are widely used to describe the evolution of a natural system (receptor), and they allow the role of other parameters to be considered, such as subsidence in the final landscape analysis (Marquenie and de Vlas, 2005; Syvitski et al., 2009; Taramelli et al., 2013a,b, 2014a).

The action of natural hazards is the 'cause' of disturbance when they drive disruption and losses, and their action is simultaneously the 'effect' of disturbance when it produces changes in the main pattern of vegetation after extreme events (Evans et al., 2004; Passalacqua et al., 2013; Van Wesenbeeck et al., 2008). Subsidence in this context can be considered a complex source of alterations in the steady states of a system; therefore, a reference state of a subsiding ecosystem must be defined spatially and temporally (Taramelli et al., 2013a,b). Although the spatial influence of subsidence can be wider than the specific area of interest because of subsequent flooding and erosion, it can be defined with different levels of precision based on the spatial scale of observation.

When referring to ecosystem functions such as vegetation gain and loss, the temporal scale becomes increasingly important because the steady state of a subsiding vegetated ecosystem must be fixed (D'Alpaos et al., 2012; Marani et al., 2006; Taramelli et al., 2014b; Temmerman et al., 2007).

Temporal observations include defining the disturbance typology that can be considered as chronic or continuous and specific conditions of disturbance that generate perturbation or stress. A continuous rate of subsidence determined at large temporal scales shows adapted vegetation with species that are resistant to altitude variation; however, at a shorter temporal ranges such as groups of rainless years, the intervention of higher rates of subsidence can drive the extinction of some of the most sensitive species (Taramelli et al., 2011; Van Dobben and Slim, 2005, 2012).

Moreover, subsidence in dynamic ecosystems such as coasts can sometimes represent the continuous inputs required to maintain the viability and organisation of living components. This means that there are ecosystems in a non-equilibrium state that are responding continuously to environmental gradients (rainfall, subsidence) and ecological interactions (competition and extinction e Taramelli et al., 2014b). Normal forcing and processes become disturbances when the nominal bounds are exceeded (Corenblit et al., 2011; Pimm, 1984). Therefore, the challenge is not only in determining how subsidence is a cause and effect disturbance but also in establishing when a normal forcing becomes a disturbance by establishing thresholds. Another aspect in analysing the feedback between subsidence and costal vegetation is that disturbances are not strictly negative phenomena; when disruptive events free resources or open corridors for species cross-changes, the biodiversity and stability of communities can increase (Reinhardt et al., 2010). Stress is an effect of disturbance and can be considered a specific perturbation characterised by specific variations from the steady state induced by the propagation of disturbance (Antonellini and Mollema, 2010; D'Alpaos et al., 2012; Marani et al., 2010; Wang and Temmerman, 2013). These phenomena occur both for natural and anthropogenic reasons that may have a synergic effect and increase the total displacement for heavily populated coastal lowland areas in particular. Natural subsidence that results from autocompaction of sediment under its own weight is enhanced by sub-surface fluid withdrawal, drainage and ground over- burden that increase the potential for inundation, coastal erosion, habitat disruption and salt-water intrusion. As summarised by Chen and Rybczyk (2005), coastal subsidence in these depositional zones is a function of five processes: (1) down warping, (2) tectonic activity, (3) consolidation of Tertiary, Pleistocene, and Holocene deposits, (4) shallow subsidence, and (5) underground water and gas extraction (Taramelli et al., 2014a). When only natural processes are considered, the combination of 1, 2, and 3 defines deep subsidence, and shallow and deep subsidence combined equal the total subsidence (Cahoon et al., 1995; Tosi et al., 2012).

Improvements by new monitoring techniques that produce more accurate results by remote sensing have increased the study of the spatial and temporal evolution of this phenomena and allowed the construction of a series of simulation models designed to reduce risks to the environment. As stated by Hung et al. (2010), considerations when selecting a monitoring system are a 1) high spatial

sampling density, 2) good measurement accuracy and 3) high temporal frequency. However, the selection is usually made according to the available funding. Various methods have been used for measuring and mapping the spatial gradients and temporal rates of regional and local subsidence and horizontal ground motion (Galloway et al., 1999; Tosi et al., 2013). The methods generally measure relative changes in the position of the land surface, and the observable position is typically a geodetic reference mark that was established so that any movement can be attributed to deep-seated ground movement rather than surficial effects.

Interferometric synthetic aperture radar (InSAR) analysis (Bamler and Hartl, 1998; Rosen et al., 2000) is a remote sensing technique that takes into account a multi-temporal systematic acquisitions and wide spatial coverage; these features make them particularly useful for regional monitoring, such as what is required for the analysis of coastal areas. Therefore, this technique has been discussed in a large number of publications, and practical applications have been developed for coastal environments. In particular, urban and peri-urban coastal areas have been extensively studied with this technique, with case studies such the Venice Lagoon, the Nile River Delta, Taiwan, New Orleans (Bock et al., 2012; Hung et al., 2010) and Indonesia, where the subsidence rate was clearly related to groundwater and gas extraction using the InSAR method (Chaussard et al., 2013). InSAR exploits SAR data, which can be divided into 2 main categories: 1. large coverage area (100 km) and long revisiting time (35 days); 2. small coverage area (40 km) and short revisiting time (4e11 days). ERS and Envisat belong to the first category, whereas Cosmo Sky Med and TerraSar-X belong to the second.

In coastal areas, SAR-based techniques, such as interferometric SAR (interferometric synthetic aperture radar (InSAR)), persistent scatterer interferometry (PSI), permanent scatterer (Ferretti et al., 2001), SBAS (Berardino et al., 2002), and interferometric point target analysis (IPTA) (Strozzi et al., 2003), are integrated into a Subsidence Integrated Monitoring System (SIMS) to overcome the limits characterising each technique. The Venice Lagoon is an area where SIMS efficiently merged the different displacement measurements obtained by high precision-levelling, differential and continuous global positioning system (GPS) data, and synthetic aperture radar (SAR)-based interferometry to obtain information on land deformation from 1992 to the present (Tosi et al., 2009; Chaussard et al., 2013).

In this paper, the use of data from the “Extraordinary Plan of Environmental Remote Sensing” by the Italian Ministry of Environment (Ministero dell'Ambiente e della Tutela del Territorio e del Mare e MATTM) shows that the PSInSAR technique integrated with a SBAS temporal analysis and can produce extremely accurate (mm per year) results in vertical resolution that are consistent with the results obtained by other absolute measurement techniques, such as GPS and topographic levelling.

2. Description of the study area

2.1. Geologic, geomorphologic and hydrogeological settings

The Foce Bevano is a small fluvial outlet located in the northern Adriatic near the town of Ravenna (Fig. 1). The Bevano is a river with a catchment area of 92.5 km^2 (Balouin et al., 2006) and total length of 34 km. The site is located in a densely populated area (south of the Po Delta) that is also one of the most important natural environments along the northern Adriatic coast where natural geomorphological dynamics control a non-urbanised stretch of approximately 5 km. The river mouth is characterised by ecologically important habitats, such as wetlands, pinewoods, sandy beaches and sand dunes. This relatively minor watercourse forms a small-scale estuarine system because the tidal excursion is limited along the Italian coasts, so large-scale estuaries are almost absent.

Over the past 50 years, the Bevano area has undergone major morphological changes (Armaroli et al., 2013), which has allowed the study of its evolution and dynamics. In particular, its mouth underwent a rapid northward migration as a result of the dominance of marine processes, such as alongshore currents, coupled with a low energy fluvial regime. During these years the river mouth has been loosing hydraulic efficiency, also because the river has become completely controlled and flooding avoided. This has led to the prevalence of marine processes at the mouth, with the outlet behaving essentially as a tidal inlet, seasonally closed especially after storms (Balouin et al., 2006; Sedrati et al., 2011). Moreover, the channel migration caused a rapid erosion of the dunes located immediately north of the mouth. Therefore, an intervention of artificial stabilisation was necessary along the trench of coastline. In 2006, the mouth of the river was closed and reopened 500 m south (Gardelli et al., 2007), while the dredged sand was used to reconstruct dunes. Since then the system has been reasonably stable, also because the northern bank is partially protected by environmentally friendly timber training structures. Only minor works of repairs were done in the last few years (Ciavola et al., 2012).

In the stratigraphic classification, the deposit outcropping of the post-evaporite succession is part of the Supersynthem Emiliano- Romagnolo, which is the stratigraphic unit that includes the late-Quaternary sediments of the Po Plain (Ricci Lucchi et al., 1982). This Supersynthem includes the Sintema Emiliano-Romagnolo Inferiore (AEI) and the Sintema Emiliano-Romagnolo Superiore (AES) (Cibin et al., 2005). The AEI is the oldest part of Super-synthem; however, it is not present in any of the outcrops. In contrast, the AES represents the upper portion of the Superynthem, and all of the continental sediment outcroppings can be identified. Climatic and eustatic fluctuations have conditioned the sedimentary dynamics in Northern Adriatic (Correggiari et al., 2005). In effect, the

subsoil contains the cyclic alternation of organic clays, silts, sands and gravels. The AES is divided into additional subsynthems that correspond to recent deposits that are related to the transgressive and regressive sea phases that occurred during the Quaternary (Cibin et al., 2005). The Modena Unit (AES8a) emerges in the mouth of the Bevano River and represents the top part of the Ravenna Subsynthem (AES8). The AES8a is composed of surficial and more recent sediments, including those currently in progress, which are several metres thick (maximum 10 m).

The Ravenna Subsynthem consists of fluvial gravels covered by clay, silt and sand that have a tabular geometry and average thickness of 25e30 m. The top of the Ravenna Subsynthem coincides with the topographical plan, and the basal portion is characterised by the presence of sediments rich in organic matter (Cibin et al., 2005). The origin of these sediments dates to the late Pleistocene in the post-Wurmian glaciation. From the documentation of its subsurface geology, which is available in the geognostic database and the work of AQUATER (1988) and ITER (1989), the Ravenna stratigraphy is composed of alternating layers of sand, silt and organic matter.

The stratigraphy can be summarised as follows:

- up to 10 m, there is an alternation of sandy layers with thin layers of silt and peats;
- from 10 to 25 m, the clayey silts become sandy silt with increasing depth; and
- from 25 to 30 m depth, there are silt clays and clayey silts with rare coarse sandy lenses.

According to Regione Emilia-Romagna & ENI-AGIP (1998), the Sintema Emiliano-Romagnolo Superiore (AES) hosts 4 main aquifer complexes: A1, A2, A3, and A4. Above these aquifers is a shallow unconfined aquifer (A0). In detail, the hydrogeology of the coastland is characterised by a multi-layered aquifer system confined between aquitards. The sediments related to the transgressive and regressive sea phases constitute the aquifers and aquitards. The aquifers are composed primarily of sandy lithotypes, whereas the aquitards are composed of silty-clay sediments. Fig. 2 shows the distribution of deep aquifers in the Foce Bevano area as proposed by Regione Emilia-Romagna & ENI-AGIP (1998). Data from the groundwater monitoring network of ARPA Emilia Romagna show that the deep coastal aquifers of the Ravenna coastland before the 1980s were heavily used for industrial and agricultural pumping. The pumping of an aquifer produces both elastic and inelastic land compaction (Meinzer, 1928; Jacob, 1940; Cernica, 1995; Domenico and Schwartz, 1998; Sun et al., 1999). In a hydrogeological system comprised of aquifers separated by aquitards (silty-clay sediments), such as in the Ravenna coastland (Fig. 2), the lowering of pore water pressure induced by groundwater withdrawals allows the fine-grained particles to compress or compact (Poland, 1984). The compaction process of aquitards may continue long after the stabilisation of drawdowns (Galloway et al., 1999). If the pore-water pressure recovers (e.g., withdrawals are stopped), the elastic

compaction can be gradually recovered; however, the inelastic compaction becomes permanent (Sun et al., 1999; Galloway et al., 1999). Data from the pumping well (RA36-00, 500 m from the dunes; see Fig. 2 for the localisation) show that since the early 1980s, the reduction of pumping allowed the deep aquifer to recover approximately 16 m; by the late 1990s, the depth was 6 m. The piezometric data refer to the A3 deep confined aquifer (Fig. 2) (Regione Emilia-Romagna & ENI-AGIP, 1998). Based on this evidence and considering all of the piezometric data available in the Ravenna coastland, a general rise of the potentiometric surface was observed after the 1980s (Fig. 4c). The piezometric data are consistent with the rising of groundwater levels in the Ravenna coastland discovered by Teatini et al. (2005) in which the potentiometric surface induced by the well closures that occurred after 1980s produced a pore pressure recovery in the coastal multi aquifer system. After the well closures, the rates returned to similar levels as registered before World War II (Carbognin and Tosi, 2003; Teatini et al., 2005).

3. Data sources and methodology

The basic methodology uses an RS time-series to analyse the (a) subsidence trends in coastal evolution over time and (b) time series of spatial patterns in coastal vegetation for improved ecosystem analyses. Specifically, the methodology considers examples of properties that are the best proxy for characteristics of emerged and shallow submerged coastal areas by combining multi-sensor space-borne remote sensing (SAR and optical). (Table 1).

A data set of Landsat TM and ETMþ imagery (from U.S. Geological Survey) was acquired to analyse the main spatial and temporal patterns of change that characterise the study site. Based on archive availability (Table 2), the covered time span ranged from 1991 to 2011 for Bevano (Fig. 4). The radiometric calibration and conversion from digital numbers to exoatmospheric reflectance were performed according to Chander and Markham (2003) and Chander et al., 2009 to normalise for variations in illumination conditions and solar irradiance and compensate for seasonal variations in Earth-Sun distance.

As a result of the widespread subsidence phenomena affecting the area (Taramelli et al., 2013a,b), an additional time-series of SAR (synthetic aperture radar) data (ERS-1/2 satellites e Table 3) was collected from Foce Bevano from 1993 to 2000 (Table 4), and we produced deformation maps of coastal morphology through the small baseline subset (SBAS) algorithm (Berardino et al., 2002). To validate these results and quantify the evolution of the subsidence trend in the following temporal interval (2003e2010), we also used additional interferometric data contained in the “Extraordinary Plan of Environmental Remote Sensing” by the Italian Ministry of Environment (Ministero dell'Ambiente e della Tutela del Territorio e del Mare e MATTM). The database consists of

231 deformation measurement points obtained from a time series of 90 ERS1-ERS2 and ENVISAT
232 images (acquired from 1992e2000 and 2003e2010, respectively) and calculated using the PSInSAR
233 (Permanent Scatterers) technique (Ferretti et al., 2001).
234 The interferometric data consist of a database of deformation measurement points obtained from the
235 processing of satellite images (ERS1-ERS2 and ENVISAT) acquired from 1992e2000 and
236 2003e2010, respectively. The overlap of the PS distribution on the geographical bases produces a
237 first interpretation phase, which is
238 the identification of zones in motion (unstable areas). All of the deformation measurements are
239 classified according to their displacement velocities measured along the line of sight (LOS), and they
240 are relative because the deformation is calculated with respect of a reference point position; therefore,
241 the measurements are considered stable and validated by comparing with the available GPS
242 measurements. The measured displacement represents the difference between the PS position during
243 the reading and the acquired reference. The processing allows for the determination of the
244 deformation velocity of each target, which assumes a linear model of deformation in the time. In the
245 mouth of the Bevano, the permanent scatterers correspond to existing structures that are man-made
246 (roads, buildings, roofs, and metal structures) or natural points that are stable in time (rock outcrops,
247 debris and slopes).
248
249 *3.1. Trends in coastal evolution over time: DInSAR analysis for subsidence detection*
250 *3.1.1. SBAS-DInSAR data analysis and measurement of active ground deformation in the Bevano*
251 *area*

252 To investigate the present deformation rates at the Bevano study site, we adopted the multi-temporal
253 differential interferometric SAR (synthetic aperture radar) technique. The classical technique
254 differential SAR interferometry utilises SAR image data to calculate the ground surface movements
255 that eventually occur between two different passes of a satellite over the same area, and it is based on
256 the radar concept, which is the phase of the radar signal that is returned as the satellite conveys
257 quantitative information on changes in the sensor-to-ground distance (range) caused by de-
258 formations of the surface (Bürgmann et al., 2000). By subtracting the phase of the two images and
259 then simulating and subtracting the phase contribution that results from the topographic relief (a DEM
260 is required), a differential interferogram is formed that contains the ground deformation signal that
261 occurred in the interval between the two passes (Massonnet and Feigl, 1998). The DInSAR technique
262 measures the phase changes between two separate acquisitions of the same area in similar geometric
263 conditions. With this technique, it is possible to identify any differences as a result of deformation
264 phenomena, topography or atmospheric disturbances (Massonnet and Feigl, 1998). The objective is

to isolate the phase contributions that result from actual surface movements from the contributions caused by disturbance. The phase difference in the electromagnetic wave is key to identifying the areas subject to surface movements. The accuracy of surface movements measured by the DInSAR technique depends on various factors (atmospheric effects, orbital effects, stability of ground scatterers, unwrapping errors, etc.); however, in favourable cases, the accuracy of the displacement measures can be up to a centimetre (Hanssen, 2001). The SBAS technique needs a high number of coregistered SAR data to work with differential interferogram series, which are characterised by a small spatial distance between orbital positions (spatial baseline). This geometric constraint limits the spatial decorrelation and topographic errors (Zebker and Villasenor, 1992). Through a series of differential interferograms, it is possible to obtain a velocity map of deformation and displacement time series. This technique allows quantifying average displacement per annum per each coherent pixel with accuracy on the order of millimetres (Berardino et al., 2002; Lanari et al., 2004).

In this work, we used the small baseline subset (Berardino et al. (2002) algorithm. By using SBAS, we exploited the large amount of SAR data acquired by the ERS-1/2 satellites of the European Space Agency (ESA) since 1992 to estimate the displacement time-series and mean velocities of coherent areas of the ground (Tolomei et al., 2013). The SBAS concept utilises a large number (several tens) of radar images to reduce the various noise components of DInSAR interferograms and increase the accuracy of the displacement measurements. Initially the operator defines the acceptable temporal and orbital separations occurring between the images of each DInSAR interferogram to be generated. Then, a consistent number of differential interferograms are generated using a DEM of comparable resolution and unwrapped to generate the actual displacement maps. Then, the reference pixel that will be used by all of the calculated displacements and velocities is selected, and the singular value decomposition (SVD) technique is used to invert the unwrapped phases to retrieve the displacement time series at each image date for each pixel showing a coherence value larger than a fixed threshold. The SVD algorithm is used to compute the matrix pseudoinverse to solve the over-determined linear equation system. During this step, the orbital residual and topographic errors are estimated and then subtracted. Finally, double filtering in time and space is conducted and the short-term atmospheric contribution is removed. In our SAR data processing, only the pixels showing an interferometric coherence larger than 0.7 over a minimum of 35% of the total number of the interferograms were considered reliable (Bürgmann et al., 2000). In fact the coherence value is a quality marker for each pixel because states how much a target keeps stable its physical characteristics and therefore its response to the radar impulse. So, for each retained pixel with 80 80 m dimensions on the ground, a time series of the ground displacements was calculated. All of the displacements were relative to the reference pixel (or area), which was assumed to be stable in the image (Bürgmann et al., 2000) and

along the sensor line of sight (LoS). It is important to highlight that for each pixel on the surface we obtain displacement measurements along the satellite Line of Sight with very high accuracy (resolution) up to 1e2 mm. The retrieved displacement represents the difference of the distance between the target and the sensor position at the two acquisition times (Bürgmann et al., 2000; Massonnet and Feigl, 1998).

We applied the SBAS technique to a data set of 36 ERS-1/2 images acquired on the descending pass in the period from 10/5/1992 to 29/12/1999 (Track 122, Frame 2704). We applied a multilooking process because radar images are affected by a form of noise that degrades the quality of the image itself (speckle). Averaging over the range and/or azimuth resolution cells may generate multilook images. The subsequent improvement in radiometric resolution from the multilooks causes an associated degradation in spatial resolution. In our case, we adopted a number of looks equal to 20 in the azimuth direction and 4 in the range direction. Finally, for the generation of the DInSAR couples, we imposed a maximum orbital separation of 300 m to reduce the spatial decorrelation and a maximum temporal distance between two passes of 1 000 days to limit the effects of temporal decorrelation; using these constraints, 85 interferograms were generated. We used the SRTM DEM for the topography subtraction (http://www2.jpl.nasa.gov/srtm e Farr et al. (2007)) with a ground posting of 80 80 m per pixel.

3.1.2. PSInSAR data set of active ground deformation in the Bevano area

The displacement time series, which were provided by the Italian Ministry of Environment through the Extraordinary Plan of Environmental Remote Sensing, were calculated using the PSInSAR (permanent scatterers) technique (Ferretti et al., 2001). This technique was based on observations of the phase-stable pointwise targets called permanent scatterers (PS), which were detected through a statistical analysis of the amplitudes of their electro- magnetic returns. The PS outputs included the average displacement rates over the observed period and time series of the deformation per each point with a high coherence of the area, and they provided information on the temporal evolution of the displacements. The average displacement rates were measured along the sensor's line of sight (LoS) and calculated with respect to the position of a ground reference point, which was considered to be stable over time and with coordinates known through GPS measurements. The measured displacement was the difference between the PS position in each image with respect to the reference acquisition. The processing allowed for the determination of the deformation velocity of each target, assuming a linear model of deformation in time.

The space-time characterisation of ground deformations was achieved through the displacement time series. This analysis evaluated the deformation trend of individual PS and extended beyond the

information obtainable from the velocity values alone (MATTM, 2009). For the period 1992e2010, the displacement time series was derived through a standard analysis that involved the use of a linear model to describe the target movements (T.R.E., 2008). The time series showed the displacements measured in mm along the LoS for a given PS as a function of the time elapsed since the first reference acquisition.

3.2. Time series of spatial patterns in coastal vegetation

3.2.1. Spectral mixing analysis (SMA)

Among the processing techniques, one of the most suitable in heterogeneous environments is spectral mixing analysis (SMA) because of its quantitative results on the fractional abundance of pure components within each pixel. It represents the spatial variation below the sensor resolution without assigning each pixel to a single class, such as in "hard" classifications (Taramelli et al., 2013b).

SMA is a technique that can consider sub-pixel variation in surface components. The methodology is based on the observation that radiances from surfaces with different 'endmember' reflectances usually mix linearly in their proportion to the area of the field of view. Therefore, if a limited number of distinct spectral endmembers can be found, it is possible to define a mixing space where mixed pixels can be described as linear mixtures of these endmembers. SMA allows for the estimation of the endmember fractions that best fit the observed mixed reflectances (Boardman, 1989; Small, 2004).

3.2.2. Change detection analysis from NDVI and SMA

We applied a univariate image differencing technique (Coppin et al., 2004; Lu et al., 2004; Singh, 1989) to assess the type, strength and spatial pattern of changes as described by each remotely sensed imagery. From each Landsat image, we derived the normalised difference vegetation index e NDVI (Goward et al., 1991), which was calculated as the ratio between red and near infrared radiance [NDVI 1⁄4 (NIR RED)/(NIR þ RED) where NIR (i.e., Landsat band 4) and RED (i.e., Landsat band 3) are the amounts of the near-infrared and red light, respectively, that are reflected by the vegetation and captured by the sensor of the satellite]. NDVI is recognised as an important index of ecological relevance (Kerr and Ostrovsky, 2003), and its relationships with vegetation productivity, which is the fraction of absorbed photosynthetic active radiation intercepted (fAPAR), biomass and phenological patterns are well documented (Pettorelli et al., 2005). For each interval, a new image was obtained based on a standardised difference (Zurlini et al., 2006a, 2006b) between NDVIt1 and NDVIt2, which are the NDVI images at time t1 and t2.

The NDVI change over time is a continuous variable; to obtain a binary (i.e., change, no change) map, a threshold of change must be defined; in this study, it was set to a percentile of 10% (5% on

366 each tail) of the empirical standardised difference distribution according to Zurlini et al. (2006a,
367 2006b). Whenever a pixel value in
368 DNDVIt1,t2 was less than the 5% percentile of positive values, it was marked as a change.
369 In addition to a change detection analysis using NDVI, a fraction of the vegetation from SMA has
370 been used to obtain a concurrent change detection analysis. The aim was to obtain a more sensitive
371 detection of changes to solve the signal of mixed pixels, which consist of several reflectance elements
372 that depend on the physical composition of the investigated surface and not just the absorbed
373 photosynthetically active radiation intercepted by plants. This approach provides a powerful tool for
374 deciphering the information contained inside each pixel, and it can isolate changes in natural (e.g.,
375 halophytic) vegetation from changes in classes (e.g., agricultural lands).
376
377 *3.2.3. Trend analysis (EOFs)*
378 To characterise the temporal trends in vegetation, a time series of vegetation fractions (obtained from
379 the spectral mixing analysis) was analysed to discriminate the interannual signal of vegetation
380 changes in both space and time. To this end, empirical orthogonal functions (EOFs) (Lorenz, 1956;
381 Bjornsson and Venegas, 1997; Hannachi et al., 2007; Taramelli et al., 2013a,b) have been applied. In
382 signal processing, this method includes the decomposition of a signal or data set in terms of
383 orthogonal functions, which allow us to determine the spatial patterns of change and their variation
384 and evolution over time. In addition, it can provide a quantitative measure of the contribution of each
385 of these patterns to the overall multi-temporal change. The aim is to isolate the different components
386 contributing to change within the time series and assign a value of relative importance to each one of
387 them.
388 Change detection measures the variation in vegetation cover between two instances by subtracting
389 two discrete values, and the EOF analysis can quantify spatial variability patterns and their temporal
390 evolution year by year while also providing a measure of the importance of each pattern with respect
391 to the whole time-series. The EOF analysis of the vegetation fraction maps allowed us to investigate
392 the main trends of evolution in the decades of interest.
393 To perform this analysis, we produced a spatio-temporal matrix in which each row corresponded to
394 one year (image acquisition) in the time series and each column was a time series of each pixel
395 (fraction value). In each row, we listed the vegetation fraction values associated with all of the pixels
396 of each image in the analysed time span. The second step was to calculate a new matrix by multiplying
397 the matrix by its transposed matrix. The new matrix was detrended (its mean was subtracted), and the
398 eigenvectors and eigenvalues were then calculated. The eigenvectors corresponded to the empirical
399 orthogonal functions, and the eigenvalues represent the variance associated with each eigenvector

and give a measure of the importance of each EOF to the total changes over the entire period of time. The outputs are a dimensionless map of change in the study area, and the expansion coefficients represent the evolution of the phenomena during the time period. The time evolution of an empirical orthogonal function shows how the pattern obtained in the analysis oscillates in time. The evolutions of EOFs in time are referred to as expansion coefficients, which are uncorrelated in time. The analysis of the expansion coefficients led to the identification of peaks, both positive and negative, in the vegetation evolution over the time series. We thus applied a change detection to these smaller time frames, or particular years of interest, to quantify the vegetation changes.

4. Results

4.1. Subsidence using PSInSAR and SBAS

The retrieved ascending mean velocity map from SBAS is shown in Fig. 3a in which the image pixels are symbolised as points.

Because of the low relief, diffuse vegetation cover and scarcity of rock outcrops, the level of temporal coherence is rather low in the area, and only a few pixels reach the minimum coherence level of 0.7. During the processing, all of the displacement time series are calculated with respect to the position of a ground reference point, which is considered to be stable over time and with coordinates known through GPS measurements. We selected such a reference area near flat areas where no geomorphological evidence of long-term subsidence could be found (Teatini et al., 2005; Taramelli et al., 2013a,b). The surface movements measured using DInSAR techniques are always scalar measurements along the line of sight of the satellite (Bürgmann et al., 2000). In our case (ERS imagery), the LoS is inclined approximately 23° from the vertical and looks to the east from the ascending orbit, i.e., a line running N13 W.

Our results (Fig. 3a) indicate that from 1992 to 2000, the ground in the central and upper part of the Bevano moved away from the satellite with rates of up to 5-8 mm/year, whereas the nearby areas located outside of the Bevano limits were relatively stable. From the field observations and geological setting, the main horizontal component of the movement was perpendicular to the main flat direction, whereas a negligible deformation occurred along the direction of the slope. Such movements that occur almost parallel to the ascending orbit cannot be resolved in DInSAR interferograms because they only cause a small change of distance between the SAR antenna and ground (Bürgmann et al., 2000). Therefore, we can safely assume that the displacements resulting from our SBAS analysis represented the projection in the LoS of the vertical component of ground deformation, and we can calculate the actual vertical displacement or velocity by simply dividing the LoS value by 0.9 (cosine of the local incidence angle).

In Fig. 3b and c, we show the average displacement velocities for the permanent scatterers in the Po Delta and adjoining coast from the ERS-1/2 and ENVISAT dataset. The results show that in both maps, the PS located along the coast and near the river outlets have higher displacement rates compared to inland areas, which are relatively stable. In the 1992-2000 period, the PSInSAR velocities are consistent with our SBAS results, and the measured rates are comparable in both methodologies. Both results support the findings that the Bevano area moved away from the satellite, whereas nearby areas were relatively stable. In addition, the PSInSAR results for 2003-2010 show an increase in the rate of negative displacement when compared with the period 1992-2000. In fact, in the 2003e2010 ENVISAT dataset, a large number of unstable PS are found to move away, with rates between 19.5 and 6.6 mm/year. A detailed analysis on the Bevano outlet between 2003 and 2010 confirms the trend towards negative velocities (Fig. 4b). The resulting total displacement trend, considering both PS, indicates a lower of the ground of approximately 80 mm occurred from 1992 to 2010. The retrieved displacement represents the difference of the distance between the target and the sensor position at the two acquisition times (Bürgmann et al., 2000; Massonnet and Feigl, 1998). It is important to highlight that for each pixel on the sur- face (spatial resolution) we obtain displacement measurements along the satellite Line of Sight with very high accuracy (resolution) up to 1-2 mm in the retrieved vertical displacement. Further details on the causes that produced the increase of ground subsidence in the last decade are discussed in the Discussion section.

4.2. Change detection from NDVI and SMA

The NDVI change detection in Foce Bevano from 1991 to 2011 led to a map with no extensive areas of change and sparse vegetation patches where gains and losses in biomass occurred (Fig. 5). Near the mouth and along the meandering course of the river, relatively unstable riparian and halophile vegetation areas can be detected. For both the riparian and pine forest vegetation classes, the majority of pixels shows no change (81.56% and 91.86%, respectively), whereas vegetation increased by 7% and 1%, respectively.

Change detection using SMA led to the identification of a higher number of gain and loss pixels, where they were classified as “no change” pixels using only the NDVI (Fig. 6).

Therefore, the Bevano area appears more strongly changed in terms of halophilic and riparian vegetation. The loss and gain values are consistent with the results obtained from the NDVI-based analysis and correspond to the high degree of change that occurred in the mouth region during the last two decades. To calibrate the particular value of gain and loss of vegetated areas that corresponds to the subsidence areas, we examined the distribution of values at numerous locations where a high

subsidence rate in the period 1993e2000 was found. This multi-temporal analysis showed higher displacement rates in which wetland hydrology is more strongly influenced by anthropic activities. At these sites, 9% of the loss in total vegetation value served as an accurate threshold for delineating the signature of the vegetation loss within the subsidence pixels.

The spatial component of the first EOF in Foce Bevano shows that the areas affected by major changes in vegetation distribution are those located along the coast and near the river outlet (7a). The graph of the temporal component, which represents 77% of the dataset variance, shows that the trend is affected by strong fluctuations in the initial period of analysis between 1991 and 1994 and between 1996 and 1998. The peak in 1998 may be correlated to the beginning of the accelerated subsidence rates in the area, which is shown in the InSar time series analysis.

The second EOF in Foce Bevano, which explains approximately 3% of the total variance, shows the greatest variation patterns around the mouth of the river (Fig. 7b). Its temporal component shows a more cyclical trend that becomes greater in amplitude between 2003 and 2006 when the most rapid migration of the mouth occurred, which led to the destruction of more than 150 m of dunes and part of the pinewood (Armaroli et al., 2013). To notice also the occurrence of an exceptional storm in September 2004, which, as documented by Ciavola et al. (2007) caused widespread erosion of the beach-dune system in the area north of the Bevano. The capacity of recover of vegetated communities is evident by the inverted trends observed after the 2006 intervention. As already detected through NDVI, this is clear evidence of a colonisation process that resulted from the pioneer vegetation of dunes (helped by experimental plantation during BEACHMED e Regione Emilia Romagna “Foce Bevano: l'area naturale protetta e l'intervento di salvaguardia”). Vegetation resilience may also have been favoured by the significant reduction of pumping water activities from multi- layered aquifers (Fig. 4c).

The analysis of the EOF3 (explaining 2.5% of the total change) and its expansion coefficient show an interesting trend that repeats following the same pattern within each decade (Fig. 7c).

The change map shows how variations occurred in the coastal zone, with some pixels of riparian vegetation along the river Bev- ano as well as in the river outlet that could be related to an impact of groundwater salinity (Antonellini and Mollema, 2010).

Based on the results highlighted above in the change detection for the whole time span, we investigated the distribution of vegetation change phenomena at a higher temporal resolution (inside each decade and/or in between the peaks detected from the empirical orthogonal functions).

In Foce Bevano, change detection was repeated for the two decades separately: for 1991e2001 and 2001e2010. In the first decade, it is evident that major losses in vegetation cover affected the outlet, terminal stretch of the river, areas located behind the dunes and dunes and produced an overall loss

of 21% in vegetation cover in the whole image. These changes in vegetation confirm the strong changes in the morphology of the river mouth and its rapid northern migration. The change detection map of the second decade, however, shows a 9.7% increase in vegetation cover on the dune system and river outlet; these findings may be explained by the stabilisation work carried out in 2006, which was performed by re-vegetating the dunes to increase their stability (Fig. 8) with the objective of preventing further dune and beach loss. The change in scarce vegetation cover of the dune system may, in fact, facilitate wave run-up flow and accelerate the washover sedimentation processes (Sedrati et al., 2011).

5. Discussion

The purpose of this study has been to identify phenomena and causes (natural and anthropogenic) that contribute to a lowering of the topography of the Ravenna coastal area and Bevano River mouth in particular, which experienced migration in the last de- cades. Subsequent to the intense human activity in recent decades, the alarming situation has caused the public administration to adopt new monitoring technique to manage the coastal subsidence. In areas where intense mining activity (freshwater or hydrocar- bons) occurs, the subsidence rates are higher than a metre per century. The results obtained from the present study through the PSInSAR technique, indicate increasing displacement rates after 1998 (approximately 7e9 mm/year); before 1998, the velocity was approximately 3e5 mm/year in the 1992e1998 period, which is close to the values disclosed by the ARPA-Emilia Romagna. The increase of settlement trends registered at the end of the 1990s (Fig. 4c) is associated with the activation of gas extraction from the Angela-Angelina platform in the "A.C27.EA" concession area.

Fig. 9 shows the annual gas production from the A.C27.EA concession area, which is characterised by offshore platforms located approximately 2 km from the coast (Angela Cluster and Angela Angelina. The data were collected from the official website of the Ministero dello Sviluppo Economico of Italy (UNMIG, http:// unmig.sviluppoeconomico.gov.it). With reference to Fig. 9, before 1997, the mean annual gas production was approximately 342 M Smc (data computed for the 1980e1996 period). After 1997, the Angela-Angelina platform was activated and a peak of gas production occurred in 1998 (1 748 M Smc). After 2000, the pro- duction was gradually reduced and in 2013, the values were close to those extracted before 1995 (approximately 400 m Smc).

According to Gambolati (1998), the subsidence areas caused by the methane extraction from the Angela-Angelina platform is manifested in a range of 4-5 km from the extraction field; therefore, the study area may have been influenced by human activity. The subsidence trend registered in 1998 should have continued in the subsequent years, even after the drastic decrease of methane extraction

534 that has occurred since 2004: this aspect, which was highlighted by Baù et al. (2000), represents a
535 key point because the concession area should operate through 2027 at least. Because the subsidence
536 trend registered in recent years has not been as heavy as in past decades, the reduction of gas field
537 production and groundwater withdrawals suggests a stabilisation or slight decrease of subsidence
538 rates in the next decades, at least for those induced by human activities.
539 The overall results suggest that the presence of anthropogenic activities along the coast can strongly
540 affect natural subsidence dynamics and lead to subsidence phenomena with rates and timing almost
541 incomparable to the natural trends; therefore, a non negligible effect on the coastal environment is
542 triggered. Specifically, the mouth of the river Bevano, which until 2005 was one of the few outlets in
543 the Emilia-Romagna coast that was not regimented by artificial embankments (Gardelli et al., 2007)
544 highlights numerous abandoned meanders near the beach within the time series analysis near the
545 outlet, with the last meander showing a marked northern migration that ran parallel to the coast. The
546 rapid migration that occurred in recent decades is mainly attributable to subsidence of the river mouth,
547 which can be seen from both ana- lyses (PSInSAR and EOF techniques). The validity of the data and
548 results confirms that the subsidence rates obtained with SAR interferometry for the period 1992-2000
549 are consistent with the general subsidence trend in the Ravenna coastal area for both natural and
550 anthropogenic causes. In the mouth of the river Bevano, previous studies by Carminati and Martinelli
551 (2002) and Teatini et al. (2005) recorded a total subsidence of 90 cm from 1897 to 1992, which was
552 based on geometric levelling data derived from IGM campaigns. In particular, subsidence peaks were
553 found between 1950 and 1980 in which both methane extraction and water withdrawal occurred
554 (Carminati and Martinelli, 2002). After this date, the reduction of groundwater extraction led to a
555 significant decrease of subsidence rates. As shown in Figs. 4c and 9, when the groundwater extraction
556 was reduced (potentiometric surface gradually recovered from the 1980s) an increase in natural gas
557 extraction occurred in August 1998. Because of several appeals in 2004, a gradual decrease in gas
558 production was observed. The displacement time series between 1992 and 2010 indicated a land
559 subsidence of approximately 80 mm. The mean velocities syn- thetically represent the general pattern
560 of ground deformation; however, the time series exhibits nonlinear components shown by the change
561 of slope, which is indicative of the presence of different linear trends (Fig. 4c). Two distinct trends
562 can be identified; from 1992 to 1999, the displacement was limited to less than 20 mm and could be
563 related by both natural and anthropogenic causes (Bertoni et al., 2005) and from August 1998, a
564 steeper slope indicated a faster displacement that resulted from the contemporary beginning of
565 methane extraction in the “Angela-Angelina” platform (4 km NE of Foce Bevano). Despite the
566 reduction in gas extraction starting in 2004 (Fig. 9) and the recovery of potentiometric surface as a
567 result of the stoppage of pumping wells, the displacements remained roughly the same from 1998 to

2010 (approximately 9 mm/year). In general, the displacement rates appear to have reached high values that were not as high as the values registered in the past when both the groundwater and gas extractions were operating. According to Teatini et al. (2005), from 1972 to 1977, a subsidence rate of approximately 45 mm/year was registered in the Bevano area according to levelling surveys.

In addition, our multi-temporal analysis shows that for a given location with high subsidence rates, the surrounding area shows vegetation losses consistent with the negative evolution of the coastal stretch. Most of these locations correspond to areas subject to anthropic pressure and show a high correlation with pumping activities that exacerbated the subsidence problem. At these sites, 9% of the loss in vegetation represents a threshold value to delin- eate the signature of vegetation loss within the subsidence pixels. There is also a correspondence between the peaks in the first two EOFs (Fig. 7b and c) and main trends in the displacement time series (Fig. 4c). The two vegetation peaks in 1998 and 2004 for EOF1 and EOF2, respectively, may represent the vegetation's response to the impacts of a faster subsidence trend, which re-started in 1998 likely as a result of the increase in methane extraction. The results compared with previous studies highlight that both the depth of the water table from the surface and water salinity are very important factors in controlling vegetation distribution, with a high density where the water table is deep (approximately 1.5 m or more) and salinity is low (Antonellini and Mollema, 2010). These measurements in the dune slacks and estuaries indicate a signifi- cant relationship between salinity degree, vegetation species richness and subsidence rates. A decrease in plant species richness and density occurs in the coastal vegetation when a subsidence rate threshold is exceeded (6 mm/year). Results show that a generally small loss of vegetation has been observed. However, a decrease in the total vegetation amount was observed, and this is the opposite of the change expected based on its relation with elevation (an increase). Management of the vegetation presence will thus need to take into account each of these factors, based on specific habitat and species richness conservation objectives dealing with extreme event. Wetland reclamation, groundwater pumping for agricultural and industrial purposes, and methane extraction near the coast are among the main causes of anthropogenic subsidence (Van Dobben and Slim, 2012; Chaussard et al., 2013). The coastal area could be particularly impacted by accelerated subsidence, which often results in higher flooding frequencies in low-lying areas. The work conducted on the dune system between Lido di Dante and Foce Bevano has detected a general degradation of the dunes between 2001 and 2009 (Ciavola and Armaroli, 2010; Sedrati et al., 2011; Armaroli et al., 2012). Across this period, an exceptional storm occurred in September 2004, which triggered an erosion phase not compensated according to Gardelli et al. (2007) that was not balanced by sediment injection through replenishments, which could explain some of the patterns observed in the first and second-order EOF components.

6. Conclusions

This research shows that remote sensing methods are effective in analysing variability and the resulting uncertainties in several parameters of relevance to flooding. The feedback between the climatological, biophysical and morphological parameters illustrated here are not only conceptual but are one of the first attempts to quantitatively evaluate different physically remote sensing- based models at a local to regional scale. The results emphasise that using hierarchical remote sensing vegetation pattern models over time can demonstrate how the morphology of different sub- systems represent a balance between inputs (forcing agents such as climate) and natural responses (related single changes such as vegetation evolution). Moreover, the temporal evolution morphology (e.g., subsidence rate) also influences the temporal evolution produced by the different vegetation parameters identified for the study sites. Considering the extrapolation of the historical trends shown by the different approaches, the possible future evolution including uncertainties, are highlighted. The PSInSAR technique may be a useful tool for the Authority in charge for the management of the land subsidence to check preliminarily,

in the case of a possible further request of the extension of the concession licence, the critical withdrawal in terms of expected anthropic subsidence and its effect on coastal area. Moreover, the analysis of subsidence trend allows to understanding the response time between the increase of methane withdrawals and the acceleration and magnitude of subsidence rates. This approach, coupled with the fact that recent Italian law (DM 9 Agosto 2013) does not allow the exploration and exploitation of new gas fields under 12 miles from the coastline, may be considered a key instrument to limit further geomorphological and environmental problems along the northern Adriatic coast. The considerations here obtained may be of such utility to understand and to manage the effects, which can be triggered in geologically similar area, affected by heavy groundwater and methane extractions. Therefore, we suggest that the ground velocity subsidence rate maps obtained using DInSAR techniques and integrated to the multispectral endmember fraction maps can provide a quantitative parameter to improve the monitoring approach for coastal areas. Being the observations by PSInSAR technique acquired at about monthly scale over extensive areas, the subsidence phenomenon can be evaluated step by step relating it with vegetation variation and changes. The occurrence of soil subsidence in coastal areas can be used then as a case study to mimic sea level rise and its effects on vegetation. The Bevano test area represents an ideal test case because of substantial coastal estuary areas and subsidence due to water pumping and gas extraction activities.

Acknowledgements

636 The support of the European Commission through the projects THESEUS (Contract 244104) and
637 MICORE (Contract 202798) are gratefully acknowledged. Permanent Scatter data were from the
638 PROGETTO PSI: Progetto Persistent Scatterers Interferometry (PSI) Ministero dell'Ambiente-
639 Portale cartografico Nazionale (http://www.pcn.minambiente.it/GN/progetto_psi.php?lan1⁄4it#).
640 Data provided by the European Space Agency and USGS.
641
642
643 **References**
644 Antonellini, M., Mollema, P., 2010. Impact of groundwater salinity on vegetation species richness in
645 the coastal pine forests and wetlands of Ravenna, Italy. Ecol. Eng. 36, 1201-1211.
646 AQUATER, 1988. Caratteristiche idrogeologiche, idrauliche ed idrodinamiche della falda freatica e
647 rapporti falda freatica-subsidenza nelle pinete di S. Vitale e di classe (RA). Comune di Ravenna
648 (Italy). Technical Report (in italian).
649 Armaroli, C., Ciavola, P., Perini, L., Lorito, S., Valentini, A., Masina, M., 2012. Critical storm
650 thresholds for significant morphological changes and damage along the Emilia-Romagna coastline,
651 Italy. Geomorphology 143-144, 34-51.
652 Armaroli, C., Grottoli, E., Harley, M.D., Ciavola, P., 2013. Beach morphodynamics and types of
653 foredune erosion generated by storms along the Emilia-Romagna coastline, Italy. Geomorphology
654 199, 22-35.
655 Balouin, Y., Ciavola, P., Michel, D., 2006. Support of subtidal tracer studies to quantify the complex
656 morphodynamics of a river outlet: the Bevano, NE Italy. J. Coast. Res. (SI 39), 602-607.
657 Bamler, R., Hartl, P., 1998. Synthetic aperture radar interferometry. Inverse Probl. 14, R1-R54.
658 Baù, D., Gambolati, G., Teatini, P., 2000. Residual land subsidence near abandoned gas fields raises
659 concern over Northern Adriatic Coastland. EOS, Trans. Am. Geophys. Union 81, 245-252.
660 Berardino, P., Fornaro, G., Lanari, R., Sansosti, E., 2002. A new algorithm for surface deformation
661 monitoring based on small baseline differential SAR interferograms. IEEE Trans. Geosci. Remote
662 Sens. 40 (11), 2375-2383.
663 Bertoni, W., Elmi, C., Marabini, F., 2005. The subsidence of Ravenna. Giornale di Geologia
664 Applicata 1, 23-32.
665 Bjornsson, H., Venegas, S., 1997. A Manual for EOF and SVD Analyses of Climatic Data. CCGCR
666 Report, 97(1).
667 Boardman, W.J., 1989. Inversion of imaging spectrometry data using singular value decomposition.
668 In: Proceedings of the 12th Canadian Symposium on Remote Sensing, pp. 2069-2072.

669 Bock, Y., Wdowinski, S., Ferretti, A., Novali, F., Fumagalli, A., 2012. Recent subsidence of the
670 Venice Lagoon from continuous GPS and interferometric synthetic aperture radar. Geochem.
671 Geophys. Geosyst. 13 (3), Q08011. http://dx.doi.org/ 10.1029/2012GC004270.
672 Bürgmann, R., Rosen, P.A., Fielding, E.J., 2000. Synthetic aperture radar interferometry to measure
673 Earth's surface topography and its deformation. Annu. Rev. Earth Planet. Sci. 28 (1), 169-209.
674 Cahoon, D.R., Reed, D.J., Day, J.W., 1995. Estimating shallow subsidence in microtidal salt marshes
675 of the southeastern United States: Kaye and Barghoorn revisited. Mar. Geol. 128, 1-9.
676 Carbognin, L., Tosi, L., 2003. Il progetto ISES per l'analisi dei processi di intrusione salina e
677 subsidenza nei territori meridionali delle province di Padova e Venezia. Istituto per lo Studio della
678 Dinamica delle Grandi Masse e Consiglio Nazionale delle Ricerche, Venezia (Italy), pp. 63-83.
679 Carminati, E., Martinelli, G., 2002. Subsidence rates in the Po Plain, northern Italy: the relative
680 impact of natural and anthropogenic causation. Eng. Geol. 66, 241-255.
681 Cernica, J.N., 1995. Geotechnical Engineering: Soil Mechanics. Wiley, New York. Chander, G.,
682 Markham, B.L., 2003. Revised Landsat-5 TM radiometric calibration procedures, and post-
683 calibration dynamic ranges. IEEE Trans. Geosci. Remote Sens. 41, 2674-2677.
684 Chander, G., Markham, B., Helder, D., 2009. Summary of current radiometric calibration coefficients
685 for Landsat MSS, TM, ETMþ, and EO-1 ALI sensors. Remote Sens. Environ. 113, 893-903.
686 Chaussard, E., Falk Amelung, F., Abidin, H., Hong, S.-H., 2013. Sinking cities in Indonesia: ALOS
687 PALSAR detects rapid subsidence due to groundwater and gas extraction. Remote Sens. Environ.
688 128, 150-161.
689 Chen, Z., Rybczyk, J., 2005. Coastal subsidence. In: Schwartz, M. (Ed.), Encyclopedia of Coastal
690 Science. Springer Academic Publishers, Netherlands, pp. 302e304. Ciavola, P., Armaroli, C., 2010.
691 Evoluzione recente del sistema dunale di Lido di Dante-Foce Bevano (Ravenna): fattori naturali ed
692 impatto antropico. Studi Costieri 17, 19-38 (in Italian).
693 Ciavola, P., Armaroli, C., Chiggiato, J., Valentini, A., Deserti, M., Perini, L., Luciani, P., 2007.
694 Impact of storms along the coastline of Emilia-Romagna: the morphological signature on the Ravenna
695 coastline (Italy). J. Coast. Res. (SI 50), 540-544.
696 Ciavola, P., Tondello, M., Carniel, S., Sclavo, M., 2012. Artificial deviation of a small inlet (Bevano,
697 northern Italy): prediction of future evolution and planning of management strategies using open-
698 source community coastal models. Coast. Eng. Proc. 1 (33)
699 http://dx.doi.org/10.9753/icce.v33.management.57 management.57.
700 Cibin, U., Severi, P., Correggiari, A., Roveri, M., et al., 2005. Note illustrative della carta geologica
701 d'Italia alla scala 1:50.000-Foglio 240-241 Forlì-Cervia. APAT (Agenzia per la Protezione

dell'Ambiente e per i servizi Tecnici). Dipartimento Difesa del Suolo, Servizio Geologico Italiano, p. 104.
Coppin, P., Jonckheere, I., Nackaerts, K., Muys, B., Lambin, E., 2004. Digital change detection methods in ecosystem monitoring: a review. Int. J. Remote Sens. 25 (9), 1565-1596.
Corenblit, D., Baas, A.C.W., Bornette, G., Darrozes, J., Delmotte, S., Francis, R.A., Gurnell, A.M., Julien, F., Naiman, R.J., Steiger, J., 2011. Feedbacks between geomorphology and biota controlling Earth surface processes and landforms: a review of foundation concepts and current understandings. Earth Sci. 106, 307-331.
Correggiari, A., Cattaneo, A., Trincardi, F., 2005. The modern Po Delta system: lobe switching and asymmetric prodelta growth. Mar. Geol. 222e223 (1e4), 49-74.
Domenico, A., Schwartz, F.W., 1998. Physical and Chemical Hydrology, second ed. Wiley, New York.
D'Alpaos, A., Da Lio, C., Marani, M., 2012. Biogeomorphology of tidal landforms: physical and biological processes shaping the tidal landscape. Ecohydrology 5, 550-562.
Evans, E., Ashley, R., Hall, J., Penning-Rowsell, E., Saul, A., Sayers, P., Thorne, C., Watkinson, A., 2004. Foresight: Future Flooding. Scientific Summary. In: Future Risks and Their Drivers, vol. I. Office of Science and Technology (OST), London, UK.
Farr, T.G., Rosen, P.A., Caro, E., Crippen, R., Duren, R., Hensley, S., Kobrick, M., Paller, M., Rodriguez, E., Roth, L., 2007. The shuttle radar topography mission. Rev. Geophys. 45 (2), 33.
Ferretti, A., Prati, C., Rocca, F., 2001. Permanent scatterers in SAR interferometry. IEEE Trans. Geosci. Remote Sens. 39, 8-20.
Galloway, D., Jones, D.R., Ingebritsen, S.E., 1999. Land Subsidence in the United States. U.S. Department of the Interior and U.S. Geological Survey. Circular 1182, p. 177.
Gambolati, G., 1998. CENAS: Coastline Evolution of the Upper Adriatic Sea due to Sea Level Rise and Natural and Anthropogenic Land Subsidence. Kluwer Academic Publishers, Dordrecht, p. 344.
Gardelli, M., Caleffi, S., Ciavola, P., 2007. Evoluzione morfodinamica della foce del torrente Bevano. Studi Costieri 13, 53-74.
Goward, S.N., Markham, B., Dye, D.G., Dulaney, W., Yang, A.J., 1991. Normalized difference vegetation index measurements from the advanced very high resolution radiometer. Remote Sens. Environ. 35, 257-277.
Hallegate, S., Green, C., Nicholls, R.J., Corfee-Morlot, J., 2013. Future flood losses in major coastal cities. Nat. Clim. Chang. 3, 802-806.
Hannachi, A., Jolliffe, I., Stephenson, D., 2007. Empirical orthogonal functions and related techniques in atmospheric science: a review. Int. J. Climatol. 27 (9), 1119-1152.

736 Hanssen, R.F., 2001. Radar Interferometry: Data Interpretation and Error Analysis, vol. 2. Kluwer
737 Academic Pub.
738 Hung, W.-C., Hwang, C., Chang, C.-P., Yen, J.-Y., Liu, C.-H., Yang, W.-H., 2010. Monitoring severe
739 aquifer-system compaction and land subsidence in Taiwan using multiple sensors: Yunlin, the
740 southern Choshui River Alluvial Fan. Environ. Earth Sci. 59 (7), 1535-1548.
741 ITER, 1989. Progetto esecutivo per l'adeguamento della discarica provinciale ai sensi dell'art. 1 del
742 D.L. 36/87 e alle disposizioni del D.P.R. 915/82. Technical Report (in italian).
743 Jacob, C.E., 1940. On the flow of water in an elastic artesian aquifer. Trans. Am. Geophys. Union
744 22, 574-586.
745 Kerr, J.T., Ostrovsky, M., 2003. From space to species: ecological applications for remote sensing.
746 Trends Ecol. Evol. 18 (6), 299-305.
747 Lanari, R., Mora, O., Manunta, M., Mallorqui, J., Berardino, P., Sansosti, E., 2004. A small-baseline
748 approach for investigating deformations on full-resolution differential SAR interferograms. Geosci.
749 Remote Sens., IEEE Trans. 42, 1377-1386.
750 Lorenz, E.N., 1956. Empirical Orthogonal Functions and Statistical Weather Prediction, Report no.1,
751 Statistical Forecasting Project. MIT Massachusetts Institute of Technology, Department of
752 Meteorology, Cambridge, Massachusetts.
753 Lu, D., Mausel, P., Brondizio, E., Moran, E., 2004. Change detection techniques. Int. J. Remote Sens.
754 25 (12), 2365-2401.
755 Marani, M., Belluco, E., Ferrari, S., Silvestri, S., D'Alpaos, A., Lanzoni, S., Feola, A., Rinaldo, A.,
756 2006. Analysis, synthesis and modelling of high-resolution observations of salt-marsh
757 ecogeomorphological patterns in the Venice lagoon. Estuar. Coast. Shelf Sci. 69, 414-426.
758 Marani, M., D'Alpaos, A., Lanzoni, S., Carniello, L., Rinaldo, A., 2010. The importance of being
759 coupled: stable states and catastrophic shifts in tidal biomorphodynamics. J. Geophys Res. 115.
760 Marquenie, J.P., de Vlas, J., 2005. The impact of subsidence and sea level rise in the Wadden Sea:
761 prediction and field verification. In: Vermaat, J.E., et al. (Eds.), Managing European Coasts: Past,
762 Present and Future. Springer Verlag, Berlin Heidelberg, pp. 355-363.
763 Massonnet, D., Feigl, K.L., 1998. Radar interferometry and its application to changes in the Earth's
764 surface. Rev. Geophys. 36 (4), 441-500.
765 MATTM, 2009. Linee guida per l'analisi di dati interferometrici satellitari in aree soggette a dissesti
766 idrogeologici. Ministero dell'Ambiente e della Tutela del Territorio e del Mare. Piano Straordinario
767 di Telerilevamento Ambientale (PSTA), lotto 2.
768 Meinzer, O.E., 1928. Compressibility and elasticity of artesian aquifers. Econ. Geol. 23, 263-291.

769 Nicholls, R.J., Marinova, M., Lowe, J.A., Brown, S., Vellinga, P., De Gusmao, D., Hinkel, J., Tol,
770 R.S.J., 2011. Sea-level rise and its possible impacts given a 'beyond 4°C world' in the twenty-first
771 century. Philos. Trans. R. Soc. A Math. Phys. Eng. Sci. 369, 161-181.
772 Passalacqua, P., Lanzoni, S., Paola, C., Rinaldo, A., 2013. Geomorphic signatures of deltaic processes
773 and vegetation: the Ganges-Brahmaputra-Jamuna case study. J. Geophys. Res. Earth Surf. 118, 1-12.
774 Pettorelli, N., Vik, J.O., Mysterud, A., Gaillard, J.-M., Tucker, C.J., Stenseth, N.C., 2005. Using the
775 satellite-derived NDVI to assess ecological responses to environmental change. Trends Ecol. Evol.
776 20 (9), 503-510.
777 Pimm, S.L., 1984. The complexity and stability of ecosystems. Nature 307, 321-326.
778 Poland, J.F., 1984. Guidebook to Studies of Land Subsidence Due to Ground-water Withdrawal. In:
779 UNESCO Studies and Reports in Hydrology, vol. 40. United Nations Educational, Scientific and
780 Cultural Organization, Paris, France, p. 305. Reinhardt, L., Jerolmack, D., Cardinale, B.J., Vanacker,
781 V., Wrigh, J., 2010. Dynamic interactions of life and its landscape: feedbacks at the interface of geo
782 morphology and ecology. Earth Surf. Process. Landf. 35, 78-101.
783 RER and ENI-AGIP, 1998, 119 pp., 9 sheets. In: Di Dio, G. (Ed.), Riserve Idriche Sotterranee Nella
784 Regione Emilia-Romagna. S.EL.CA., Firenze.
785 Ricci Lucchi, F., Colalongo, M.L., Cremonini, G., Gasperi, G.F., Iaccarino, S., Papani, G., Raffi, S.,
786 Rio, D., 1982. Evoluzione sedimentaria paleogeografica nel margine appeninico. In: Guida alla
787 geologia del margine appenninico padano. Guide Geologiche Regionali. S.G.I, pp. 17-46.
788 Rosen, P., Hensley, S., Joughin, I., Li, F., Madsen, S., Rodríguez, E., Goldstein, R., 2000. Synthetic
789 aperture radar interferometry. Proc. IEEE 88 (3), 333-382.
790 Sedrati, M., Ciavola, P., Armaroli, C., 2011. Morphodynamic evolution of a microtidal barrier; the
791 role of overwash: Bevano, Nothern Adriatic Sea. J. Coast. Res. ISSN: 0749-0208 (SI 64), 696-700.
792 Singh, A., 1989. Digital change detection techniques using remotely-sensed data. Int. J. Remote Sens.
793 10 (6), 989-1003.
794 Small, C., 2004. The Landsat ETMþ spectral mixing space. Remote Sens. Environ. 1e2 (93), 1-17.
795 Strozzi, T., Wegm, U., Werner, C., Wiesmann, A., Spreckel, V., 2003. JERS SAR interferometry for
796 land subsidence monitoring. IEEE Trans. Geosci. Remote Sens. 41 (7), 1702-1708.
797 Sun, H., Grandstaff, D., Shagam, R., 1999. Land subsidence due to groundwater withdrawal: potential
798 damage of subsidence and sea level rise in southern New Jersey, USA. Environ. Geol. 37, 290e296.
799 Syvitski, J.P.M., Kettner, A.J., Overeem, I., Hutton, E.W.H., Hannon, M.T., Brakenridge, G.R., Day,
800 J., Vo€ro€smarty, C., Saito, Y., Giosan, L., Nicholls, R.J., 2009. Sinking deltas due to human
801 activities. Nat. Geosci. 2, 681-686.

802 Taramelli, A., Pasqui, M., Barbour, J., Kirschbaum, D., Bottai, L., Busillo, C., Calastrini, F.,
803 Guarnieri, F., Small, C., 2013a. Spatial and temporal dust source in Northern China identified using
804 advanced remote sensing analysis. Earth Surf. Proc. Landf. 38, 793-809.
805 Taramelli, A., Valentini, E., Dejana, M., Zucca, F., Mandrone, S., 2011. Modelling coastal processes
806 by means of innovative integration of remote sensing time series analysis. In: Proc. of Geoscience
807 and Remote Sensing Symposium A. Taramelli et al. / Ocean & Coastal Management 108 (2015) 74-
808 88 87 88 A. Taramelli et al. / Ocean & Coastal Management 108 (2015) 74-88.
809 (IGARSS), 2011 IEEE International, Vancouver, BC, pp. 1547e1550. http://
810 dx.doi.org/10.1109/IGARSS.2011.6049364.
811 Taramelli, A., Valentini, E., Cornacchia, L., Mandrone, S., Monbaliu, J., Thompson, R., Hogart, S.,
812 Zanuttigh, B., 2013b. Modelling uncertainty in estuarine system by means of combined approach of
813 optical and radar remote sensing. Coast. Eng. 87, 77.96.
814 http://dx.doi.org/10.1016/j.coastaleng.2013.11.001.
815 Taramelli, A., Manzo, C., Valentini, E., Cornacchia, L., Pieralice, F., 2014a. Coastal Subsidence:
816 Causes, Mapping and Monitoring. Invited Chapter to Encyclopedia of Natural Hazards. Wiley&Sons,
817 Ltd (in press).
818 Taramelli, A., Cornacchia, L., Valentini, E., Bozzeda, F., 2014b. Non-linear power law approach for
819 spatial and temporal pattern analysis of salt marsh evolution. Earth Surf. Dyn. Discuss. 1, 1061-1095.
820 http://dx.doi.org/10.5194/esurfd-1-1061-2013.
821 Teatini, P., Ferronato, M., Gambolati, G., Bertoni, W., Gonella, M., 2005. A century of land
822 subsidence in Ravenna, Italy. Environ. Geol. 47, 831-846.
823 Temmerman, S., Govers, G., Wartel, S., Meire, P., 2003. Spatial and temporal factors controlling
824 short-term sedimentation in a salt and freshwater tidal marsh, Scheldt estuary, Belgium, SW
825 Netherlands. Earth Surf. Proc. Landf. 28, 739-755.
826 Temmerman, S., Bouma, T.J., Van de Koppel, J., Van der Wal, D., De Vries, M.B., Herman, P.M.J.,
827 2007. Vegetation causes channel erosion in a tidal landscape. Geology 35, 631-634.
828 Tolomei, C., Taramelli, A., Moro, M., Saroli, M., Salvi, S., 2013. Analysis of DGSD impending over
829 the Fiastra lake (Central Italy), by geomorphological assessment and deformation monitoring using
830 satellite SAR Interferometry. Geomorphology 201, 281-292.
831 Tosi, L., Teatini, P., Carbognin, L., Brancolini, G., 2009. Using high-resolution data to reveal depth-
832 dependent mechanisms that drive land subsidence; the Venice coast, Italy. Tectonophysics 474 (1-2),
833 271-284.

834 Tosi, L., Teatini, P., Bincoletto, L., Simonini, P., Strozzi, T., 2012. Integrating geotechnical and
835 interferometric SAR measurements for secondary compressibility characterization of coastal soils.
836 Surv. Geophys. 33, 907-926.
837 Tosi, L., Teatini, P., Strozzi, T., 2013. Natural versus anthropogenic subsidence of Venice. Sci. Rep.
838 3, 2710. http://dx.doi.org/10.1038/srep02710.
839 T.R.E, 2008. Tele-Rilevamento Europa. PSInSARTM e Manuale D'uso.
840 Van Dobben, H.F., Slim, P.A., 2005. Evaluation of changes in permanent plots in the dunes and upper
841 salt marsh at Ameland East: ecological effects of gas extraction. In: Begeleidingscommissie
842 Monitoring Bodemdaling Ameland (Ed.),
843 Monitoring Effecten Van Bodemdaling Op Ameland-Oost, pp. 1-36.
844 Van Dobben, H.F., Slim, P.A., 2012. Past and future plant diversity of a coastal wetland driven by
845 soil subsidence and climate change. Clim. Chang. 110 (3-4),
846 597e618.
847 Van Wesenbeeck, B.K., Van de Koppel, J., Herman, P.M.J., Bouma, T.J., 2008. Does scale-
848 dependent feedback explain spatial complexity in salt-marsh ecosystems? Oikos 117, 152e159.
849 Wang, C., Temmerman, S., 2013. Does biogeomorphic feedback lead to abrupt shifts between
850 alternative landscape states: an empirical study on intertidal flats and marshes. J. Geophys. Res. Earth
851 Surf. 118, 229-240.
852 Zebker, H., Villasenor, J., 1992. Decorrelation in interferometric radar echoes. IEEE Trans. Geosci.
853 Remote Sens. 30, 950-959.
854 Zurlini, G., Riitters, K., Zaccarelli, N., Petrosillo, I., Jones, K., Rossi, L., 2006a. Disturbance patterns
855 in a socio-ecological system at multiple scales. Ecol. Complex. 3(2), 119-128.
856 Zurlini, G., Zaccarelli, N., Petrosillo, I., 2006b. Indicating retrospective resilience of multi-scale
857 patterns of real habitats in a landscape. Ecol. Indic. 6, 184-204.

858
859
860
861
862
863
864
865
866
867

868 **FIGURES**

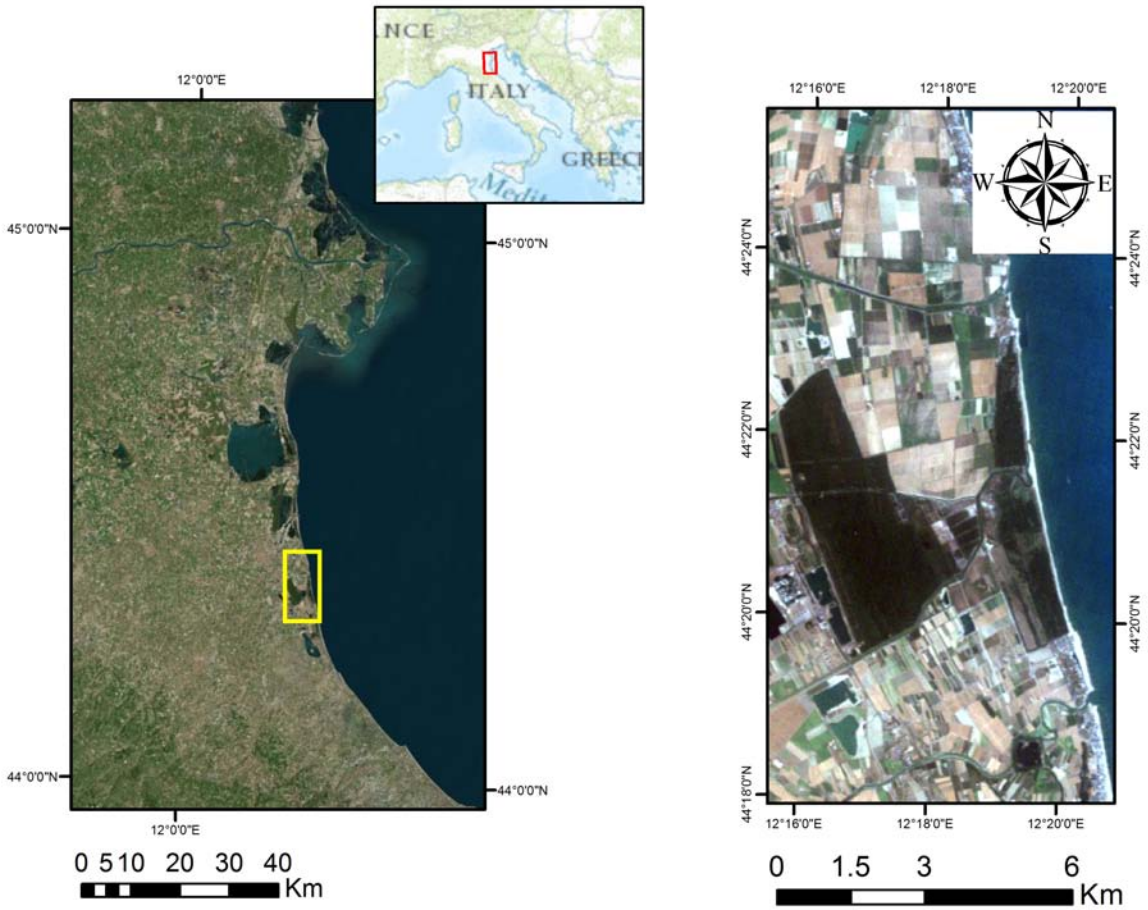

869

870 *Figure 1 - Landsat satellite image (16/07/2003) of the Northern Adriatic coast (on the left) and the study site*
871 *Foce Bevano (on the right).*

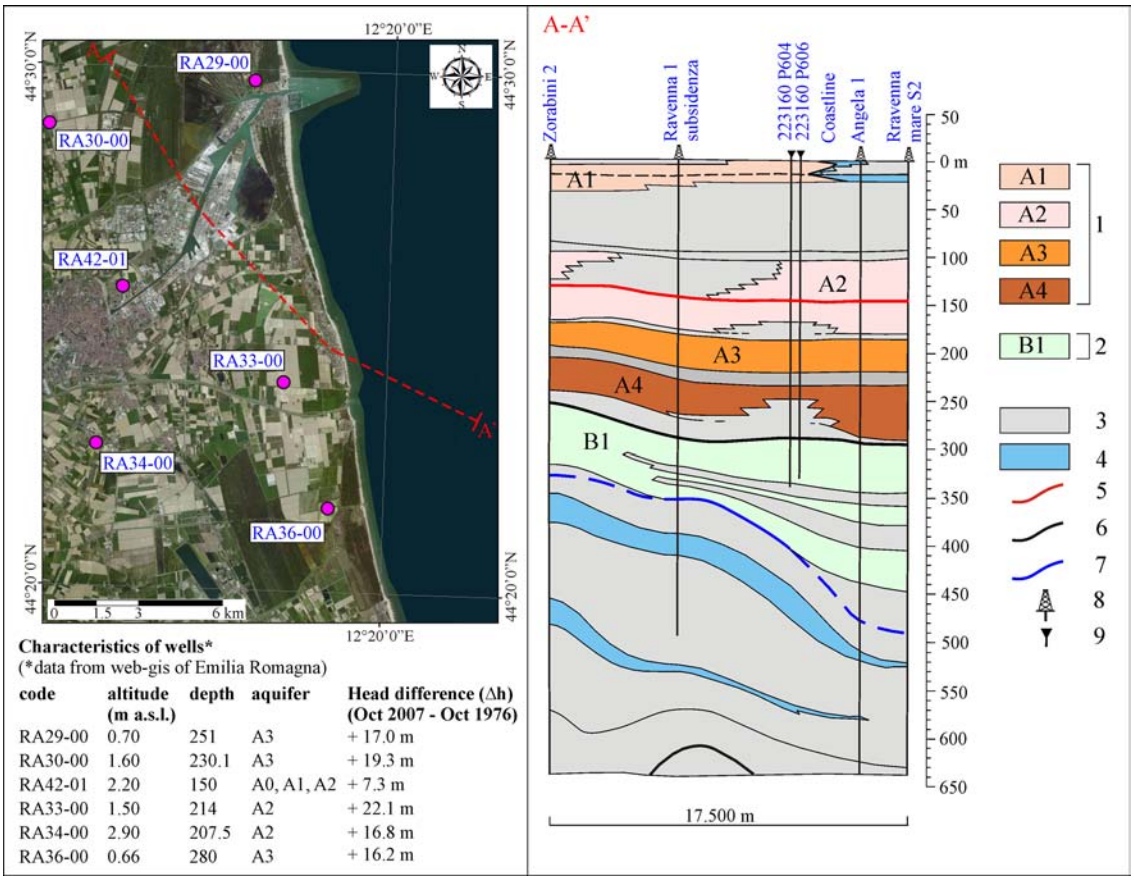

Characteristics of wells*
(*data from web-gis of Emilia Romagna)

code	altitude (m a.s.l.)	depth	aquifer	Head difference (Δh) (Oct 2007 - Oct 1976)
RA29-00	0.70	251	A3	+ 17.0 m
RA30-00	1.60	230.1	A3	+ 19.3 m
RA42-01	2.20	150	A0, A1, A2	+ 7.3 m
RA33-00	1.50	214	A2	+ 22.1 m
RA34-00	2.90	207.5	A2	+ 16.8 m
RA36-00	0.66	280	A3	+ 16.2 m

Figure 2 – Main aquifers in the Foce Bevano area with the location and characteristics of wells monitored by ARPA Emilia-Romagna. The hydrostratigraphic section is modified from Regione Emilia-Romagna & ENI-AGIP (1998). The meaning of the symbols are as follows: 1) aquifers hosted by the Sintema Emiliano-Romagnolo Superiore (A1, A2, A3, and A4); 2) highest aquifer of the Sintema Emiliano-Romagnolo Inferiore (B1); 3) aquitards; 4) salty waters; 5) Tyrrhenian transgression; 6) boundary of aquifer complexes; 7) salt–freshwater interface; 8) gas wells; and 9) water wells (piezometers).

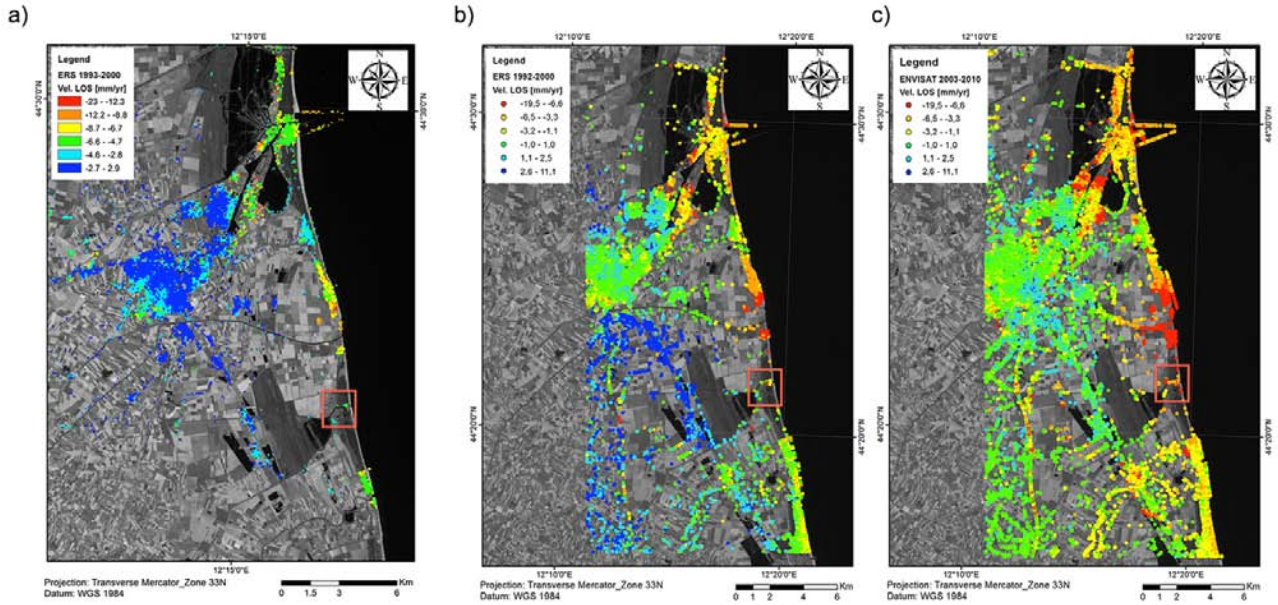

Figure 3 - (a) Ground velocity map (mm/year) of deformation calculated between 1993 and 2000 using the SBAS methodology, (b) between 1992 and 2000 using PSInSAR on ERS1-ERS2 data, and (c) between 2003 and 2010 using PSInSAR on ENVISAT data.

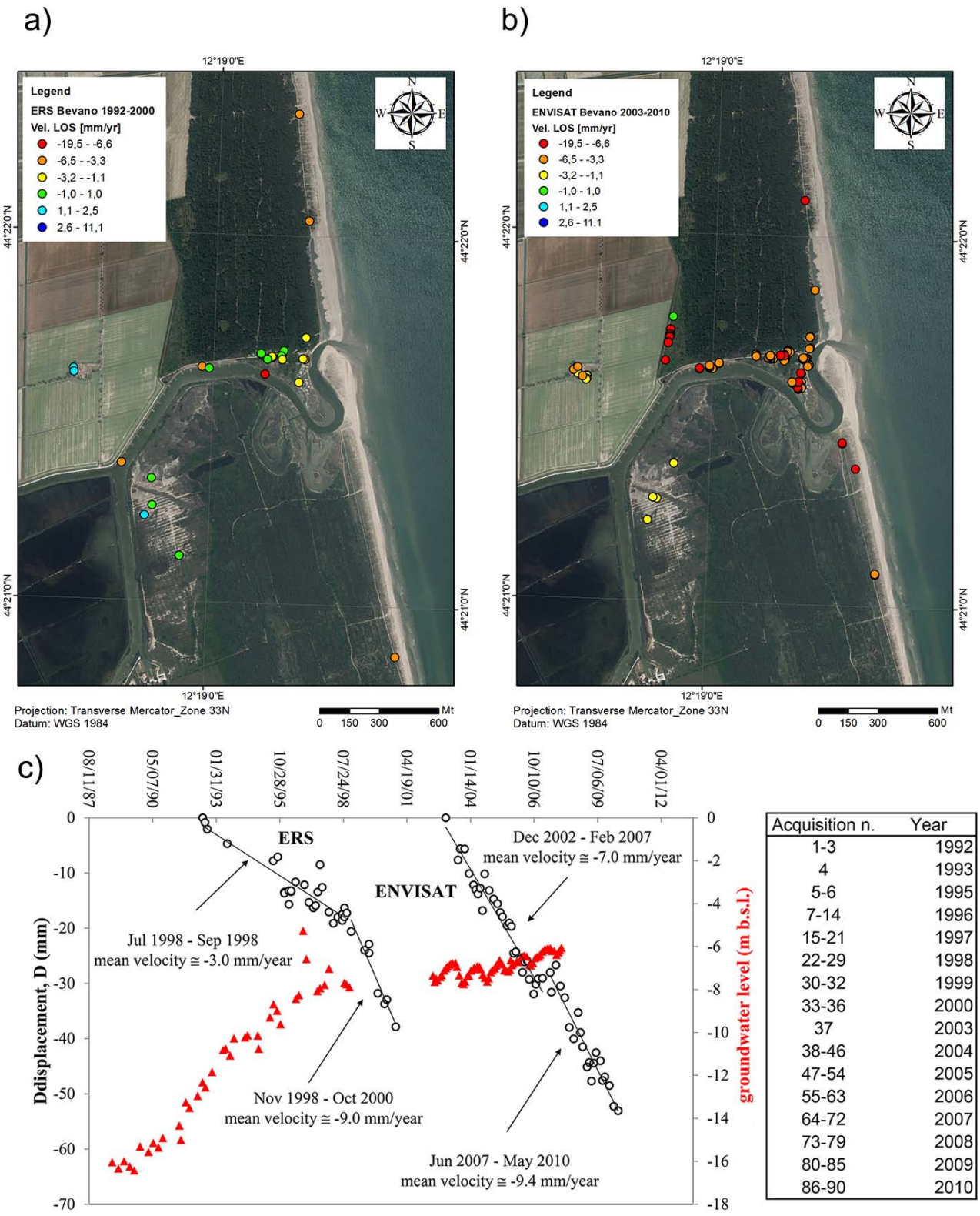

Figure 4 — Map of average displacement rates of the (a) ERS-1/2 and (b) ENVISAT PS, which were located around Foce Bevano. In the period 2003–2010, a greater number of PS is observed as moving away from the sensor with rates higher than before 1992–2000, which likely indicates an increase in terms of subsidence. (c) Piezometric level of well RA36-00 (red triangles, see Fig. 2 for localisation) and displacement time series (black circles) in Foce Bevano from 1992 to 2010.

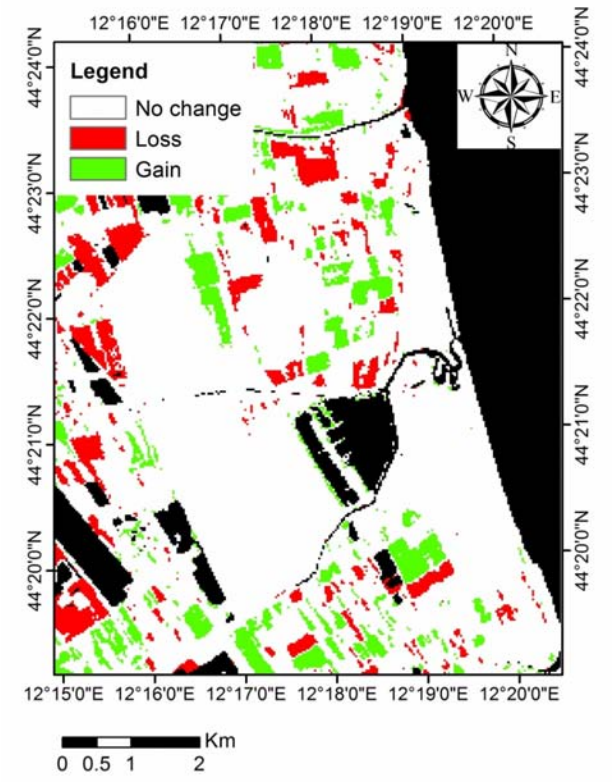

Figure 5 – Change detection in the decades 1991-2011 based on NDVI.

Figure 6 – Change detection in the decades 1991-2011 based on vegetation fraction from SMA.

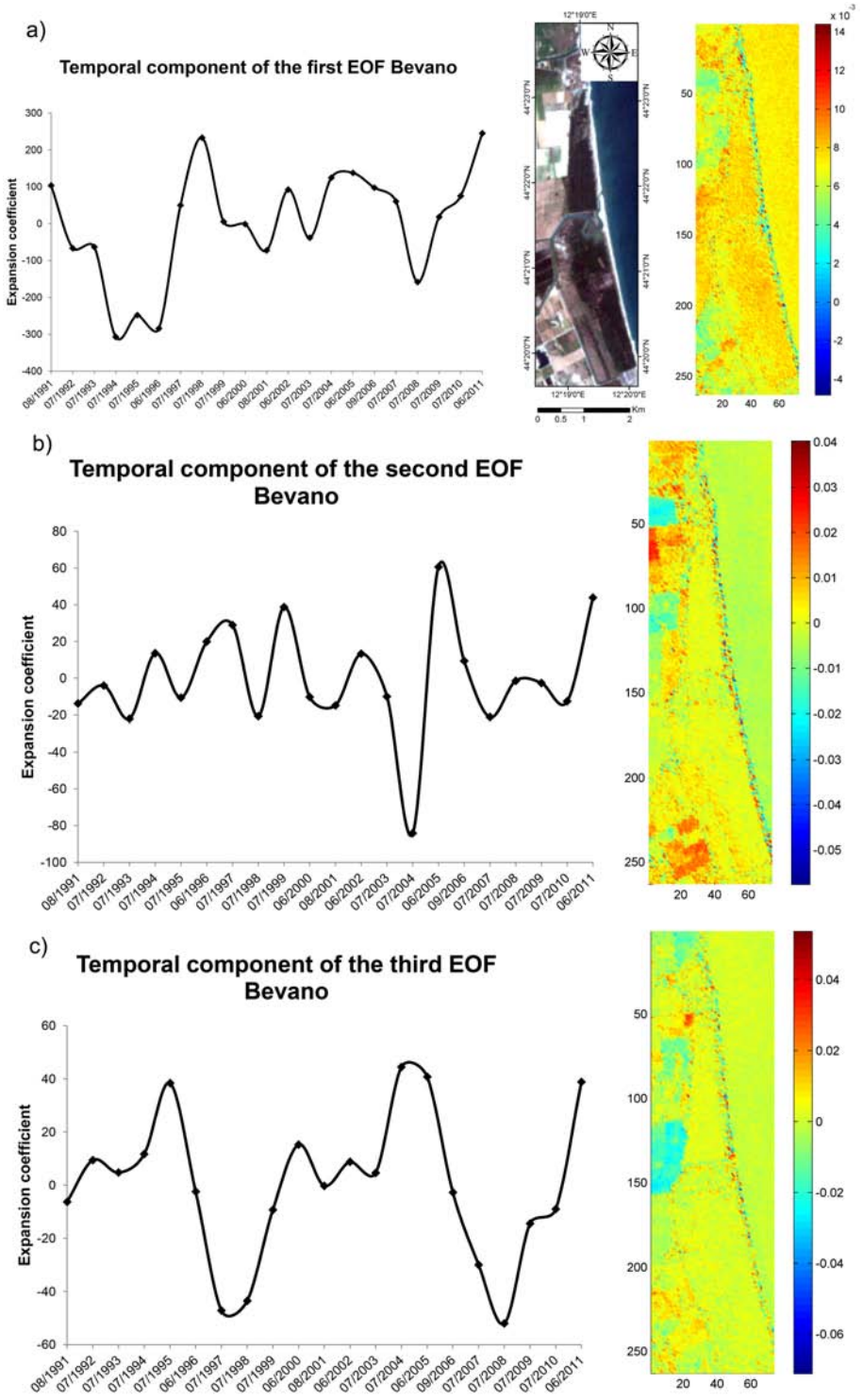

Figure 7 – Temporal and spatial component of the three EOF in Foce Bevano.

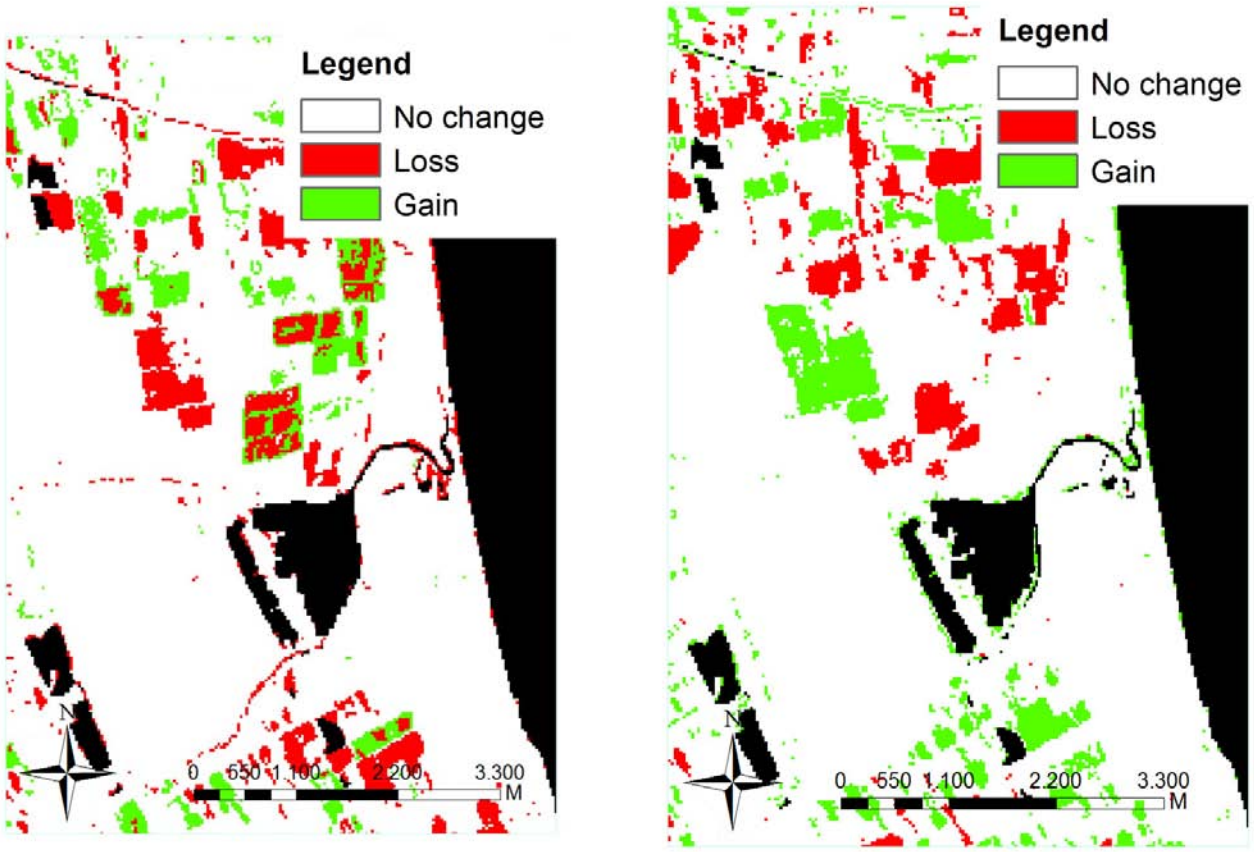

Figure 8 – SMA change detection in Foce Bevano between 2001–1991 (left) and 2010–2001 (right).

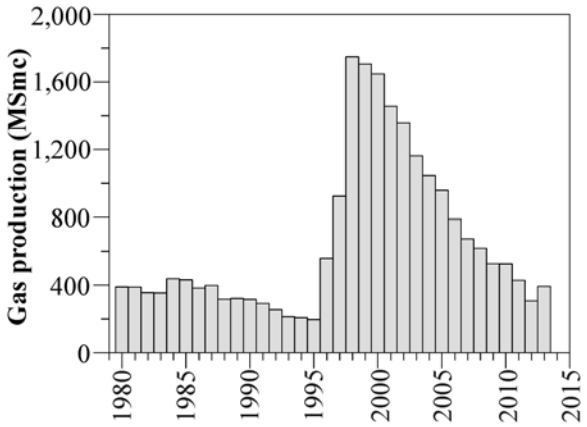

Figure 9 – Annual gas production from the A.C 27.EA concession area from 1980-2013 (data are taken from the official website of the Ministero dello Sviluppo Economico of Italy (UNMIG, http://unmig.sviluppoeconomico.gov.it).

TABLES

Table 1: Specifications of the Landsat Enhanced Thematic Mapper (ETM+) sensor (U.S. Geological Survey, 2003).

Band n.	Wavelength (μm)	Spatial resolution (m)
1	0.45 - 0.515	30
2	0.525 - 0.605	30
3	0.63 - 0.69	30
4	0.75 - 0.90	30
5	1.55 - 1.75	30
6	10.4 - 12.5	60
7	2.09 - 2.35	30
8	0.52 - 0.9	15

Table 2 – List of Landsat images used for the analysis in Foce Bevano.

Acquisition date	Sensor	Path	Row
07/08/1991	TM	192	29
24/07/1992	TM	192	29
04/07/1993	TM	191	29
14/07/1994	TM	192	29
01/07/1995	TM	192	29
01/06/1996	TM	192	29
22/07/1997	TM	192	29
18/07/1998	TM	191	29
13/07/1999	ETM	191	29
20/06/2000	ETM	192	29
03/08/2001	ETM	191	29
27/06/2002	TM	192	29
16/07/2003	TM	191	29
18/07/2004	TM	191	29
10/06/2005	TM	192	29
01/09/2006	TM	192	29
27/07/2007	TM	191	29
29/07/2008	TM	191	29
16/07/2009	TM	191	29
03/07/2010	TM	191	29
27/06/2011	TM	192	29

Table 3 –Specifications of the ERS sensors

Satellite	ERS-1	ERS-2
Launch date	17 July 1991	21 April 1995
Altitude	800 Km	800 Km
Revisiting cycle	35 days	35 days
Acquisition time	21.16 in ascending orbit 9.40 in descending orbit	21.16 in ascending orbit 9.40 in descending orbit
Orbit inclination	98.5 degree inclination orbit	98.5 degree inclination orbit
Look angle	23 deg look angle towards right	23 deg look angle towards right
Band/wavelength	C/5.8 cm	C/5.8 cm
Frame Dimension	100x100 Km	100x100 Km
SAR pixel size	12.5x12.5 m (3 looks)	12.5x12.5 m (3 looks)

923 *Table 4 – Acquisition date of the ERS-1/2 SAR images used for the SBAS technique in Foce Bevano.*

ERS-1/2 SAR	
10/05/1992	02/07/1997
14/06/1992	06/08/1997
27/09/1992	15/10/1997
01/11/1992	08/04/1998
06/12/1992	13/05/1998
21/03/1993	17/06/1998
25/04/1993	22/07/1998
12/09/1993	26/08/1998
21/11/1993	30/09/1998
02/08/1995	24/03/1999
10/10/1995	28/04/1999
28/02/1996	02/06/1999
02/04/1996	06/07/1999
07/05/1996	07/07/1999
08/01/1997	15/09/1999
12/02/1997	20/10/1999
23/04/1997	24/11/1999
28/05/1997	29/12/1999

924
925